

RFNNS: Robust Fixed Neural Network Steganography with Popular Deep Generative Models

Yu Cheng*
East China Normal University
Shanghai, China

Jiuan Zhou*
East China Normal University
Shanghai, China

Jiawei Chen
East China Normal University
Shanghai, China

Zhaoxia Yin[†]
East China Normal University
Shanghai, China

Xinpeng Zhang
Fudan University
Shanghai, China

Abstract

Image steganography is a technique that conceals secret information in a cover image to achieve covert communication. Recent research has demonstrated that Fixed Neural Network Steganography (FNNS) exhibits significant practical advantages, as it enables stable and efficient steganographic embedding and extraction without requiring neural network training. However, the stego image generated by existing FNNS methods suffers from considerable distortion and exhibits poor robustness, severely reducing the security and practicality of steganography. To address the aforementioned issues, we propose a Robust Fixed Neural Network Steganography (RFNNS). In RFNNS, we introduce a texture-aware localization technique to add perturbations carrying secret image information to complex texture areas that are less perceptible to the human eye, thereby ensuring the quality of the stego image. To enhance robustness, a robust steganographic perturbation generation (RSPG) strategy is designed, which enables slight perturbations to be accurately decoded even after common image attacks. Subsequently, the generated robust perturbations are combined with the AI-generated cover image to produce the stego image. The receiver only needs to share the secret key and employ the same decoding network structure to accurately extract the secret image from the attacked stego image. Experimental results demonstrate that RFNNS achieves enhanced performance in terms of security, including imperceptibility and anti-steganalysis performance. Furthermore, RFNNS demonstrates superior robustness against common image attacks, such as JPEG compression, Gaussian noise, and contrast adjustment, across diverse embedding capacities, outperforming existing SOTA FNNS methods.

CCS Concepts

• **Security and privacy** → Security services; Human and societal aspects of security and privacy.

Keywords

Robust steganography, Fixed neural network, Deep generative models

*Both authors contributed equally to this work.

[†]Corresponding author.

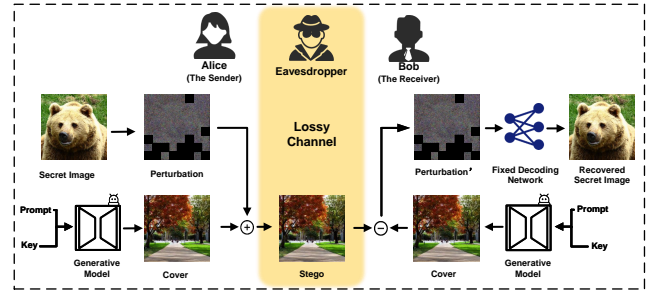


Figure 1: The Process of Sending and Extracting in RFNNS.

1 Introduction

With the rapid development of generative AI, the widespread application of generated content, such as images, has become increasingly prevalent in daily life, raising significant concerns about data security. Steganography [24, 27, 33, 34, 41, 48], a critical information hiding technique [30, 45, 57], ensures covert communication by embedding secret information in carriers such as images while remaining undetectable to humans and machine eavesdroppers, effectively safeguarding data security.

Traditional image steganography relies on the Syndrome Trellis Codes (STCs) framework [10], which minimizes distortion to ensure security. Numerous distortion measurement functions [17, 18, 26] have been designed on the basis of this framework. Recent advancements in deep neural networks (DNNs) have transformed steganography into a data-driven and learning-based approach [2, 7, 20]. However, this method faces two significant challenges: (1) it requires substantial data and computational resources to train effective neural networks; (2) the need to transmit trained models between senders and receivers prior to covert communication not only incurs storage overhead but also heightens the risk of detection by eavesdroppers, thereby compromising security.

To avoid training and transmission of steganographic networks, researchers have employed Fixed Neural Networks (FNNs) [12, 23, 28, 32] to embed and extract information. This approach leverages adversarial perturbations to modify the cover image such that the stego image can trigger a fixed-parameter decoding network to output the secret information. Covert communication can be achieved by sharing only the fixed decoding network architecture and the random seed to initialize the weights between the sender and the receiver. Nevertheless, existing FNNS methods are currently characterized by poor robustness against common image attacks, low

stego image quality, and unsatisfactory anti-steganalysis performance. These limitations severely restrict the further development of this technology.

In response to the aforementioned challenges, we propose an RFNNS method. Unlike previous FNNS methods [12, 23, 28, 32], the perturbation embedded in our approach is not global but localized within selected regions. We propose a texture-aware localization technique that introduces perturbations carrying secret information into regions with high textural complexity that are less perceptible to the human eye. In addition, we devise a Robust Steganographic Perturbation Generation (RSPG) strategy that synthesizes perturbations resilient to a variety of common image attacks while keeping the distortion introduced into the stego images negligibly low. In practical applications, the receiver employs the shared secret key to access the meticulously designed decoding network we have developed, thereby reliably extracting the secret information. The sending and extraction process is shown in the Fig. 1.

An experiment was devised to thoroughly evaluate RFNNS relative to existing FNNS methods, including visual quality, robustness, and anti-steganalysis performance. The results show that RFNNS outperforms the state-of-the-art in all three aspects. In terms of robustness, the secret images recovered by RFNNS under Gaussian-noise attacks attain an average peak signal-to-noise ratio (PSNR) approximately 4 dB higher than that of competing methods. Across all contrast adjustment scenarios evaluated, it yields an average SSIM improvement of around 2-fold, demonstrating superior robustness. These gains stem primarily from the RSPG strategy, which safeguards the various embedded perturbations attacks. Because the texture-aware localization technique confines perturbations to limited regions and narrows the gap between the stego and cover images, the proposed method consistently achieves a pronounced advantage in anti-steganalysis performance, irrespective of whether the embedding rate is high or low. Due to its combined strengths in visual quality, robustness and anti-steganalysis performance, RFNNS offers greater practical value for real-world covert communication.

Our main contributions are summarized below:

- We propose a texture-aware localization technique that embeds perturbations carrying secret information into high-texture-complexity regions, which are less perceptible to the human eye. This effectively reduces the distortion of the cover image caused by the perturbations.
- A robust steganographic perturbation generation (RSPG) strategy is designed to actively simulate potential attack scenarios that images may encounter during transmission. This strategy ensures that high-quality secret images can still be reliably extracted from the stego image after it has been subjected to common image attacks.
- The Robust Fixed Neural Network Steganography (RFNNS) method is capable of accurately extracting a secret image through a meticulously designed fixed decoding network, even after the stego image has been subjected to common image attacks. Experiments demonstrate that, compared with other state-of-the-art FNNS methods, the RFNNS method exhibits superior performance in terms of visual quality, anti-steganalysis performance, and robustness.

2 Related Work

2.1 Traditional Image Steganography

In traditional image steganography, hand-crafted embedding algorithms are typically employed to subtly modify the cover image, allowing secret information to be embedded while preserving visual quality to the greatest possible extent. Traditional image steganography methods can be broadly classified into spatial domain [6, 36] and transform domain [47] approaches. To further enhance the undetectability of stego images, researchers have proposed adaptive image steganography techniques [17]. Adaptive steganography methods are often realized within a distortion coding framework, in order to minimize a defined distortion function resulting from data embedding. One of the most influential adaptive steganographic frameworks was presented in [10], using Syndrome-Trellis Codes (STCs) to encode secret information. Subsequently, various adaptive methods have been developed, each customized according to specific distortion functions [18, 26]. Typically, to maintain a high level of undetectability, these methods restrict the embedding capacity to no more than 0.5 bits per pixel (bpp). In an effort to improve the robustness of the generated stego images for real-world applications, researchers have introduced robust steganography [8, 44, 53]. Nevertheless, this approach remains constrained by critical challenges, notably its inherently limited embedding capacity and insufficient robustness against common yet potent image attacks, thereby diminishing its practical applicability.

2.2 DNN-based Image steganography

Recent advances in DNN-based [9, 42, 50] steganography have enabled efficient embedding and extraction of secret information within cover images through specialized encoder and decoder networks. Zhu et al. [58] introduced an end-to-end autoencoder-based image steganography method. SteganoGAN [56] subsequently expanded this technology, achieving an embedding capacity of up to 6 bpp. Wei et al. [46] first proposed directly generating stego images using GANs [13] without relying on separate cover images. Huang et al. [19] optimized GAN-based steganography by introducing an adaptive GAN parameter update strategy. Tang et al. [43] decoupled adversarial attack and information hiding processes, enhancing the extensibility of the method to embed information in various multimedia carriers. Peng et al. [37] utilized the inverse process of steganographic diffusion models to design a comprehensive encoding strategy that integrates the generation of steganographic space and the embedding of data, effectively improving steganography robustness.

However, these methods typically require extensive training data and considerable computational resources. Moreover, trained steganographic networks are often large in scale, necessitating covert transmission to senders or receivers who lack any steganographic tools. To simplify this process, FNNS emerged, enabling secret data embedding and extraction by adding adversarial perturbations to cover images without additional training. Ghamizi et al. [12] proposed a steganographic approach that takes advantage of a multi-label-targeted evasion attack, encoding the secret payload as the class labels assigned to the adversarial images generated during the evasion process. Kishore et al. [23] proposed a method that

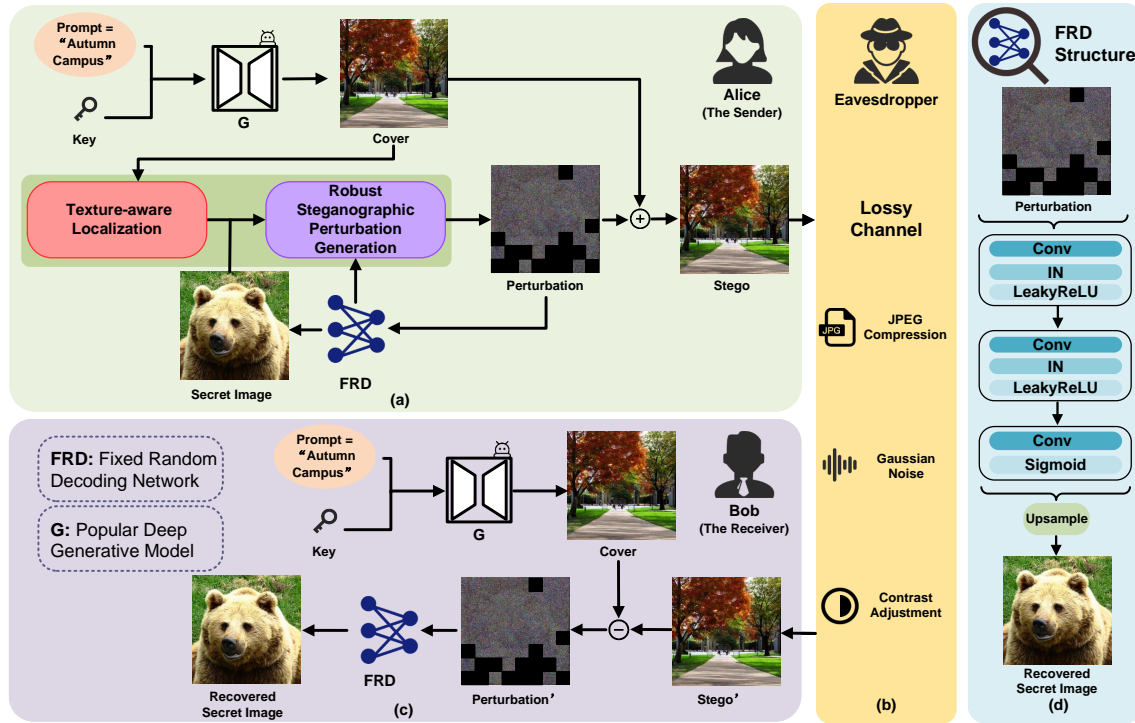


Figure 2: RFNNS framework: (a): Alice (The Sender) employs the proposed texture-aware localization technique to identify embedding regions corresponding to the perturbation. A robust steganographic perturbation generation (RSPG) strategy is then utilized to incorporate this perturbation into the AI-generated cover image, guided by a shared key, thereby producing the stego image. (b): The eavesdropping and potential image attacks that a stego image may encounter during transmission over a public channel. (c): Bob (The Receiver) first reconstructs the original cover image using the shared key to isolate the perturbation from the stego image. Subsequently, he decodes the secret image using the same decoding network. (d): Framework of Fixed Random Decoding Network.

increases embedding capacity by expanding the output dimension of the decoding network and utilizes information loss to generate encrypted images. Luo et al. [32] introduced a key-based method to synchronize steganographic tools and prevent unauthorized data recovery. Li et al. [28] proposed a Cover-separable Fixed Neural Network Steganography (Cs-FNNS) method that combines secret information with adversarial perturbations and optimizes the perturbations using a steganographic perturbation search algorithm. However, FNN-based steganographic methods often exhibit poor robustness against common image attacks, which hinders the accurate recovery of hidden information. Furthermore, these methods typically produce stego images that suffer from poor visual quality and pronounced distortion, ultimately limiting their practical applicability.

2.3 Deep Generative Models

In recent years, deep generative models—such as Generative Adversarial Networks (GANs) [13], Variational Autoencoders (VAEs) [22], Flow Models [21], and Diffusion Models [15] have advanced rapidly. Training in large-scale datasets approximates complex data distributions and has been widely used in Artificial Intelligence Generated Content (AIGC), achieving impressive results in computer vision [16], natural language processing [5], privacy protection [52], and

biological sciences [54]. For example, Rombach et al. [39] employed diffusion models to synthesize high-resolution images; Ganey et al. [11] integrated multiple models with differential privacy (DP) synthetic data generation techniques to mitigate privacy risks; and Lai et al. [25] applied deep generative models for drug molecule design, accelerating drug development and application. AIGC has also been utilized in information hiding. In RFNNS, by simply sharing a key and a prompt, both sender and the receiver can employ a generative model to produce identical cover images, thereby enabling precise localization of complex texture perturbations. Subsequently, on the basis of identified perturbation regions, we employ a RSPG strategy to embed the perturbations into specific areas of the generated cover image, thus producing a stego image. By integrating these techniques, our solution effectively enhances the practicality of covert communication.

3 The Proposed Method

In this section, we first introduce the overall framework of the proposed method. Subsequently, we detail on the texture-aware localization technique and the robust steganographic perturbation generation (RSPG) strategy. Finally, we describe the design of the decoding network.

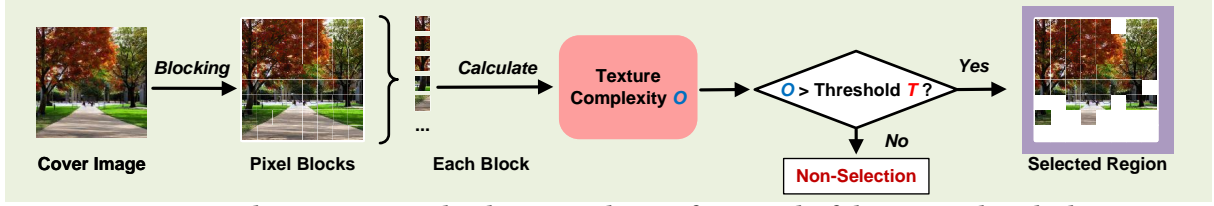


Figure 3: The texture-aware localization technique framework of the proposed method.

Table 1: Notations

Notation	Description
X_c	Cover Image $\in [0, 1]^{H_c \times W_c \times 3}$
X_s	Stego Image $\in [0, 1]^{H_c \times W_c \times 3}$
δ	Micro Perturbation $\in [0, 1]^{H_\delta \times W_\delta \times 3}$
S	Secret Image $\in [0, 1]^{H_s \times W_s \times 3}$
S'	Recoverd Secret Image $\in [0, 1]^{H_s \times W_s \times 3}$
$G(\cdot)$	Deep Generative Model
$De(\cdot)$	Decoding Network

3.1 Framework of the Proposed Scheme

In this study, we propose a novel steganography, called Robust Fixed Neural Network Steganography (RFNNS). For ease of description, the relevant symbols are shown in Table 1. Let X_c represent an AI-generated RGB cover image, with H_c and W_c denoting its height and width, respectively. The secret image to be transmitted, denoted as S , is also an RGB image with height H_s and width W_s . According to the framework depicted in Fig. 2, on the sender side, we input a secret key k_c and a shared *prompt* into a pre-trained deep generative model $G(\cdot)$ to generate the cover image X_c .

$$X_c = G(k_c, \text{prompt}) \quad (1)$$

A texture-aware localization technique is employed to identify embedding regions within the cover image. Subsequently, the secret image is transformed into subtle perturbations denoted as δ using a robust steganographic perturbation generation (RSPG) strategy with a fixed decoding network. These perturbations are iteratively updated in response to various potential attacks. The refined robust perturbations are then embedded into predetermined regions of the cover image, ultimately generating the stego image.

On the receiver side, the original cover image is reconstructed using a shared secret key k_c and a shared *prompt*. By comparing this retrieved original image with the received stego image, the receiver extracts perturbation information δ' , which has been subjected to attacks, from the predetermined embedded regions. After sharing the key for the initialization weights k_w , the receiver obtains an identical decoding network to that of the sender. By feeding the extracted perturbation δ into this network, the secret image can be accurately reconstructed from the perturbation δ' . This process can be formally described as:

$$De[k_w](\delta') = S' \quad (2)$$

3.2 Texture-aware Localization

Existing FNNS methods typically encode secret information by uniformly embedding perturbations throughout the cover image, neglecting the substantial variations in texture complexity among

different regions of the image. This uniform embedding strategy often leads to reduced visual quality and diminished anti-steganalysis performance. Considering human visual perception, subtle perturbations introduced into regions with high textural complexity are less likely to be perceptible. Therefore, embedding perturbations specifically within regions of higher textural complexity can effectively reduce the overall perturbation scale, thus enhancing the visual quality and anti-steganalysis performance.

As illustrated in Fig. 3, in practice, the cover image is initially partitioned into multiple equal-sized blocks of dimensions $b_s \times b_s$. Subsequently, the texture complexity O is computed for each block, and perturbations are introduced into the blocks whose complexity O exceeds a predefined threshold T . We employ the Local Binary Pattern (LBP) [35] method to quantify the O of each block. For every pixel $p(i, j)$ in an image block, the corresponding LBP value is calculated by comparing the grayscale intensity of the central pixel with its eight neighboring pixels. The binary value b_k for each neighbor pixel $p(i + dy, j + dx)$ is defined as follows:

$$b_k = \begin{cases} 1, & p(i + dy, j + dx) \geq p(i, j), \\ 0, & p(i + dy, j + dx) < p(i, j) \end{cases} \quad (3)$$

where (dy, dx) represents the offset of each neighboring pixel relative to the central pixel, and k ($k = 0, 1, \dots, 7$) denotes the neighbor index, arranged from left to right and then top to bottom. Following the LBP method described in [38], the resulting set of binary values b_k is used to construct an LBP histogram $H(e)$. This histogram is subsequently normalized, yielding the probability distribution $P(e)$, from which we calculate the texture complexity O as the entropy:

$$O = - \sum_{e=0}^{255} P(e) \log_2 [P(e) + \epsilon] \quad (4)$$

where ϵ a very small constant is used to avoid undefined values during the logarithmic calculation.

Once the texture complexity O has been calculated for all image blocks, blocks exhibiting O values that exceed the threshold T are marked for perturbation, as shown in the following equation:

$$\text{perturbation position} = \begin{cases} \text{chosen}, & O \geq T \\ \text{unchosen}, & O < T \end{cases} \quad (5)$$

Using this approach allows us to selectively embed subtle perturbations into blocks with higher texture complexity, thus effectively minimizing the overall perturbation scale.

3.3 Robust Steganographic Perturbation Generation

In practical steganography, transmitted images traverse complex and variable channel environments, exposing them to malicious attacks or noise interference that degrade secret information extraction accuracy. To address the aforementioned issues, a robust steganographic perturbation generation (RSPG) strategy is proposed. We aim to reduce embedding distortion and enhance anti-steganalysis performance through this strategy, while also enabling accurate recovery of the secret image from the stego image after it has undergone various image attacks.

Correspondingly, to mitigate the impact of perturbation on the quality of the cover image, the perturbation introduced during the embedding process should be as minimal as possible. We use a loss function as follows:

$$\text{loss}_1 = \text{MSELoss}(w_p, w_z) \quad (6)$$

w_p represents the generated perturbation. Here, w_z denotes a zero tensor with the same dimensionality as the perturbation, which guides the perturbation generation process to minimize distortion. Specifically, to constrain the perturbation within the limits, we use μ to bound w_p , as shown in the following formula 7.

$$w_p \leq \mu \quad (7)$$

In addition to maintaining image quality, robust extraction of secret information is critical. To accurately recover the embedded data, a second loss function is introduced:

$$\text{loss}_2 = \text{MSELoss}(S', S) \quad (8)$$

Furthermore, by simulating various attacks during the adversarial noise generation process, a loss function is designed:

$$\text{loss}_3 = \text{MSELoss}(\text{attack}_{S'}, S) \quad (9)$$

$$\text{attack}_{S'} = \begin{cases} \text{JPEG_Compression}(S, QF) \\ \text{Gaussian_Noise}(S, \rho) \\ \text{Contrast_Adjustment}(S, \eta) \end{cases} \quad (10)$$

Where QF denotes the JPEG compression quality factor, ρ represents the variance of the Gaussian noise, and η signifies the extent of contrast adjustment. This loss function actively simulates potential attacks during the perturbation generation process, thereby effectively enhancing the perturbation's robustness against common image attacks.

During the perturbation optimization process, we incorporate pre-trained steganalyzers into the later iterations to provide gradient feedback for perturbation refinement, thereby enhancing the anti-steganalysis performance of the generated stego images. Consequently, the following loss function is formulated:

$$\text{loss}_4 = \text{CrossEntropyLoss}(X_s, \text{Label}) \quad (11)$$

$$\text{CrossEntropyLoss}(X_s, y) = -\log\left(\frac{\exp(X_{s,y})}{\exp(X_{s,0}) + \exp(X_{s,1})}\right) \quad (12)$$

Label denotes the classification result provided by the steganalyzer. y denotes the current index, taking values in $\{0, 1\}$. $X_{s,0}$ represents

the logit corresponding to the classification of the image as stego image, and $X_{s,1}$ represents the logit corresponding to the classification of the image as normal.

In practice, we prioritized the visual quality of the stego images by adjusting the weight loss_1 . Empirical observations suggest that when loss_1 is reduced to a threshold L , the image distortion introduced to stego images can be almost ignored, thus preserving high visual fidelity. On this basis, we now focus on the following three objectives: the image quality of the recovered secret images, the robustness of the perturbations against channel distortions, and the anti-steganalysis performance. The refined loss function accordingly takes the following form:

$$\text{loss} = \begin{cases} L + \beta \cdot \text{loss}_2 + (1 - \beta) \cdot \text{loss}_3 + \gamma \cdot \text{loss}_4, & \text{if } \text{loss}_1 < L \\ \alpha \cdot \text{loss}_1 + \beta \cdot \text{loss}_2 + (1 - \beta) \cdot \text{loss}_3 + \gamma \cdot \text{loss}_4, & \text{if } \text{loss}_1 \geq L \end{cases} \quad (13)$$

where α , β , and γ are hyperparameters that balance the contributions of different loss functions.

The proposed strategy iteratively optimizes perturbations, ensuring both the quality of the stego images and the quality of the extracted images under common image attacks. Experimental results demonstrate that the RSPG strategy exhibits remarkable robustness and effectively meets the requirements for covert communication in practical scenarios.

3.4 Decoding Network Construction

The network architecture significantly influences decoding performance. Previous research [23, 28, 32] has demonstrated the sensitivity of decoding efficacy to architectural choices. The proposed decoding network (Fig. 2(d)) integrates convolutional (Conv) layers, instance normalization (IN), LeakyReLU activations, and a final sigmoid activation. Each Conv layer possesses learnable parameters structured as four-dimensional tensors, where the first two dimensions denote input and output channels, and the last two dimensions represent the spatial size of convolution kernels (both fixed at 3).

To enable fine-grained control over embedding capacity, convolutional layers with varied strides are strategically employed, as illustrated in Fig. 2(d). Adjusting the stride directly modifies the spatial relationship between secret information (δ/S) and the cover image (X_c), thus precisely managing different embedding capacities. After determining the design of the decoding network $D[\cdot]$ using this method and employing the shared key k_w , both the sender and receiver can independently construct identical decoding networks. This method significantly reduces the required information exchange, thus enhancing both the security and the practicality of the steganographic system.

4 Experiments

This section presents the experimental settings and results. Specifically, Section 4.1 details the experimental setup, including datasets and hyperparameters. Section 4.2 evaluates the security performance of the proposed method, while Section 4.3 focuses on its robustness in various attack scenarios. Additionally, ablation studies are provided in the Appendix to further analyze the contributions of key components.

Table 2: Stego Image Quality under Different Embedding Capacities and Attack Conditions

Capacity	Attack	Factor	Kishore et al. [23]			Li et al. [28]			Ours		
			PSNR↑	SSIM↑	LPIPS↓	PSNR↑	SSIM↑	LPIPS↓	PSNR↑	SSIM↑	LPIPS↓
1.5bpp	No Attack		24.22	0.675	0.223	41.17	0.981	0.003	41.48	0.980	0.003
	JPEG Compression	$QF=90$	14.00	0.213	1.051	25.26	0.659	0.244	25.95	0.717	0.134
		$QF=80$	13.96	0.210	1.061	23.00	0.568	0.350	25.43	0.703	0.147
		$QF=70$	13.99	0.212	1.059	22.24	0.539	0.399	22.51	0.608	0.223
	Gaussian Noise	$\rho=0.01$	14.31	0.200	0.881	30.17	0.828	0.062	32.33	0.880	0.046
		$\rho=0.04$	13.95	0.194	0.900	23.78	0.598	0.197	28.66	0.800	0.089
		$\rho=0.07$	13.93	0.193	0.890	20.72	0.471	0.323	26.72	0.748	0.124
	Contrast Adjustment	$\eta=0.9$	13.33	0.349	0.693	34.36	0.964	0.008	33.46	0.913	0.041
		$\eta=0.8$	13.08	0.389	0.643	28.88	0.934	0.015	32.98	0.899	0.043
		$\eta=0.7$	12.97	0.405	0.617	24.87	0.885	0.034	32.60	0.889	0.047
6bpp	No Attack		18.98	0.577	0.393	41.79	0.981	0.004	42.95	0.984	0.003
	JPEG Compression	$QF=90$	13.51	0.196	1.113	22.64	0.554	0.318	22.62	0.583	0.218
		$QF=80$	11.52	0.195	1.115	21.52	0.507	0.371	21.58	0.565	0.222
		$QF=70$	13.46	0.190	1.261	21.06	0.489	0.355	19.81	0.522	0.292
	Gaussian Noise	$\rho=0.01$	18.97	0.582	0.393	28.58	0.776	0.072	31.62	0.864	0.048
		$\rho=0.04$	18.75	0.568	0.418	22.58	0.551	0.208	28.51	0.786	0.087
		$\rho=0.07$	19.13	0.584	0.392	19.88	0.438	0.325	26.19	0.738	0.130
	Contrast Adjustment	$\eta=0.9$	13.75	0.428	0.579	31.68	0.914	0.017	32.73	0.908	0.043
		$\eta=0.8$	13.30	0.421	0.594	26.30	0.835	0.045	30.72	0.845	0.059
		$\eta=0.7$	13.10	0.421	0.596	22.85	0.758	0.082	28.15	0.784	0.093

4.1 Experimental Settings

Datasets. We employ a pre-trained Stable Diffusion model [39] as the generative function $G(\cdot)$ to construct a cover image dataset comprising 3,000 images, each with a resolution of 512×512 pixels. Each image is generated using a unique seed k_c and a fixed textual prompt "Campus." The resulting data set is evenly divided into three subsets, Campus-I, Campus-II, and Campus-III, each of which contains 1,000 images. These subsets are used to embed secret images randomly selected from the COCO [29], CelebA [31], and ImageNet [40] datasets, respectively. The secret images are resized to 256×256 and 128×128 pixels to accommodate high (6 bpp) and low (1.5 bpp) embedding capacities. For an embedding capacity of 1.5 bpp, the decoding network employs a convolutional kernel size of 84; for 6 bpp, the kernel size is increased to 104.

Hyperparameters. Given that JPEG compression operates in the Discrete Cosine Transform (DCT) [1] domain using 8×8 blocks, we adopt a block size of $b_s = 8$ when computing texture complexity. Empirical results indicate that this choice leads to better overall performance. To facilitate optimization, the number of image blocks is set to a perfect square, and the dimensionality of the perturbation is ensured to be no smaller than that of the secret image, allowing for more effective information extraction. Following the approach of Cs-FNNS, the total number of optimization iterations is set to 1,500. The initial learning rate is $1 \times 10^{-1.25}$, and it is halved every 500 iterations. The perturbation bound μ is fixed at 0.2. After 1,400 iterations, we incorporate pre-trained steganalysis networks, including SRNet [4] and SiaStegNet [51], to provide gradient feedback for further perturbation refinement. According to our experiments, when $loss_1$ in Equation 13 drops below 0.001, the perturbations generated have negligible impact on the visual quality of the stego image. Therefore, we set the threshold $L = 0.001$. In attack-free scenarios, the parameters in Equation 13 are configured as $\beta = 3$ and $loss_3 = 0$,

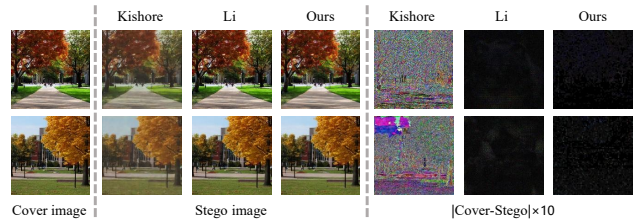


Figure 4: The image quality of stegos for different FNNS methods.

focusing optimization on information recovery. In contrast, under attack conditions, β is dynamically reduced to 0.5 to balance robustness and recovery. The remaining hyperparameters α and γ are empirically fixed at 1 and 1×10^{-5} , respectively, to ensure stable convergence while preserving secret image integrity. In Equation 5, the threshold T for texture complexity is set to 4.5. To further improve the quality of the recovered secret image, we recommend applying a lightweight post-processing denoising algorithm, such as [55].

4.2 Security

In image steganographic techniques, security is typically categorized into imperceptibility and anti-steganalysis performance.

4.2.1 Imperceptibility. Image quality is a critical metric for evaluating the imperceptibility of steganographic techniques. Fig. 4 provides a comparative visualization between the RFNNS method and two other methods in terms of the quality of recovered secret images. It is evident that the stego images generated by the proposed method are nearly indistinguishable from their respective cover images, as indicated by the almost invisible residuals magnified by a factor of 10. This result indicates that the method achieves

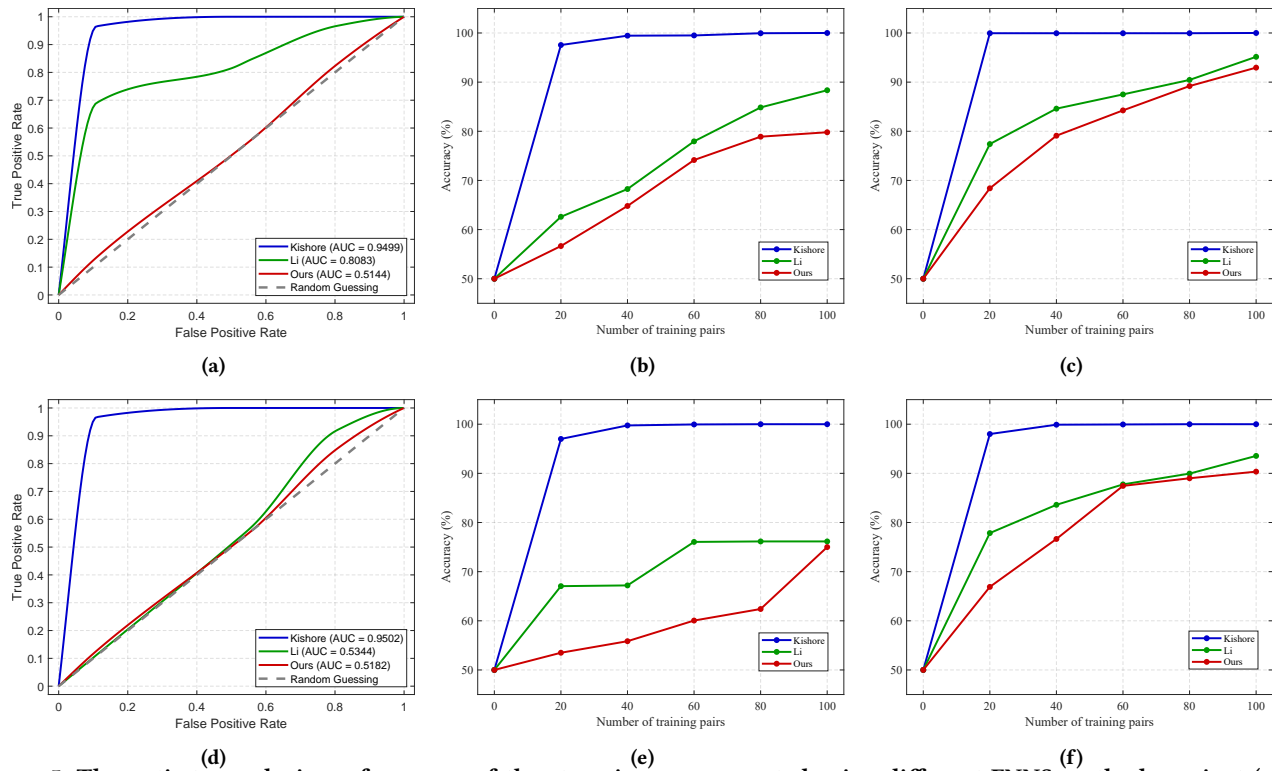


Figure 5: The anti-steganalysis performance of the stego images generated using different FNNS methods against (a) (d) StegExpose, (b) (e) YeNet and (c) (f) SiaStegNet. The top row represents low embedding capacity (1.5 bpp), while the bottom row represents high embedding capacity (6 bpp).

good color fidelity with minimal visible artifacts. As shown in Table 2, the stego images generated by RFNNS surpass those produced by other FNNS methods under both attacked and attack-free conditions. In particular, the proposed method achieves superior PSNR values in nearly all test cases. Under a 6 bpp embedding rate and a Gaussian noise condition with a variance of 0.07, the SSIM improvement reaches 68.5%, while the LPIPS metric is reduced to as low as 40% of the score achieved by the best competing method, highlighting the improved perceptual fidelity of the stego images.

4.2.2 Anti-steganalysis Performance. To assess the anti-steganalysis performance of stego images generated by different FNNS methods, we employ three widely used, publicly available steganalysis tools. The first is StegExpose [3], a conventional steganalysis tool that integrates various statistical detection methods. Furthermore, we utilize YeNet [49] and SiaStegNet [51], both of which are deep learning-based steganalysis approaches. To comprehensively evaluate the FNNS methods, each method is evaluated based on 3,000 pairs of cover / stego images. For the statistical steganalysis evaluation, we adopted the protocol from [32] by inputting all the cover / stego image pairs into StegExpose for detection. We generate receiver operating characteristic (ROC) curves for FNNS methods by varying detection thresholds within StegExpose, as illustrated in Fig. 5(a) and (d). The ideal ROC curve for steganography is represented by the diagonal green dashed line, and the optimal Area Under the ROC Curve (AUC) value is 0.5, corresponding to random guess detection. In particular, the AUC achieved by our RFNNS method is significantly lower compared to the other methods and close to this

optimal value, suggesting a high degree of undetectability against StegExpose.

Furthermore, we evaluated our approach using deep learning-based steganalyzers, YeNet [49] and SiaStegNet [51]. Before assessment, we randomly divided the cover / stego image pairs into training sets (2,000 pairs) and testing sets (1,000 pairs). Following the protocols presented in [14, 20], we train these two steganalysis networks from scratch using the training data set. Specifically, during the testing phase, we incrementally increased the number of training samples to determine how many pairs of images were necessary for effective steganalysis. Fig. 5(b), (c), (e), and (f) illustrate the detection accuracies of YeNet and SiaStegNet across varying numbers of training image pairs. According to the experimental results presented in Fig. 5, our method consistently demonstrates strong performance in detecting steganographic images. As the number of training samples increases, the detection accuracy of the steganalysis analyzer remains consistently lower than that observed with the compared methods. Specifically, with an embedding rate of 6 bpp and 100 training pairs, the detection accuracy of SRNet is limited to 75%, while that of SiaStegNet reaches 90.35%. This demonstrates the superior performance of our method in both high and low embedding capacities, particularly in scenarios involving larger training datasets.

The RFNNS outperforms existing FNNS methods in terms of imperceptibility and anti-steganalysis performance. This advantage comes from the texture-aware localization technique, which

Table 3: Recovered Secret Image Quality under Different Embedding Capacities and Attack Conditions

Capacity	Attack	Factor	Kishore et al. [23]			Li et al. [28]			Ours		
			PSNR \uparrow	SSIM \uparrow	LPIPS \downarrow	PSNR \uparrow	SSIM \uparrow	LPIPS \downarrow	PSNR \uparrow	SSIM \uparrow	LPIPS \downarrow
1.5bpp	No Attack		33.43	0.922	0.056	35.34	0.949	0.019	34.14	0.943	0.017
	JPEG Compression	$QF=90$	12.56	0.299	0.607	28.44	0.859	0.065	29.28	0.861	0.070
		$QF=80$	12.14	0.263	0.642	27.38	0.840	0.073	29.27	0.858	0.072
		$QF=70$	11.88	0.239	0.658	25.73	0.811	0.096	27.00	0.813	0.112
	Gaussian Noise	$\rho=0.01$	23.13	0.749	0.140	31.29	0.905	0.040	32.04	0.920	0.037
		$\rho=0.04$	15.90	0.517	0.392	26.27	0.811	0.101	27.44	0.816	0.124
		$\rho=0.07$	14.53	0.435	0.479	23.62	0.753	0.145	26.08	0.756	0.169
	Contrast Adjustment	$\eta=0.9$	15.05	0.440	0.478	17.41	0.562	0.382	34.62	0.968	0.016
		$\eta=0.8$	13.32	0.323	0.562	14.57	0.405	0.564	34.38	0.953	0.017
		$\eta=0.7$	12.06	0.235	0.618	13.86	0.363	0.611	33.68	0.950	0.019
6bpp	No Attack		15.69	0.472	0.491	34.61	0.938	0.027	31.09	0.910	0.058
	JPEG Compression	$QF=90$	11.65	0.227	0.690	19.53	0.686	0.263	23.60	0.720	0.253
		$QF=80$	11.55	0.223	0.695	18.45	0.651	0.311	22.85	0.696	0.260
		$QF=70$	11.45	0.218	0.699	17.54	0.617	0.362	19.24	0.572	0.411
	Gaussian Noise	$\rho=0.01$	16.35	0.495	0.451	28.85	0.851	0.083	30.07	0.855	0.117
		$\rho=0.04$	15.31	0.461	0.482	22.23	0.723	0.204	26.94	0.751	0.203
		$\rho=0.07$	14.23	0.406	0.542	19.07	0.643	0.296	24.49	0.665	0.294
	Contrast Adjustment	$\eta=0.9$	14.50	0.375	0.551	16.79	0.531	0.496	32.79	0.919	0.030
		$\eta=0.8$	13.95	0.313	0.597	15.15	0.453	0.595	30.67	0.898	0.043
		$\eta=0.7$	13.27	0.272	0.624	14.19	0.406	0.652	28.69	0.879	0.071

confines perturbation-induced distortions to minimal regions. Moreover, the RSPG strategy further ensures that the discrepancy between the stego image and its cover is kept to a low level.

4.3 Robustness

4.3.1 *Robustness under non-attack conditions.* Table 3 presents the visual quality metrics for recovered secret images generated by different methods. The proposed method is compared with existing FNNS methods in three key metrics: PSNR, SSIM, and Learned Perceptual Image Patch Similarity (LPIPS). Under non-attack conditions, the performance of RFNNS is largely consistent with SOTA methods at 1.5 bpp. In the higher capacity scenario, RFNNS maintains an SSIM value greater than 0.9, demonstrating that it continues to achieve satisfactory quality in terms of hidden information extraction. While the secret image quality achieved by RFNNS is slightly inferior to that of the Cs-FNNS method, this is mainly because the embedding perturbations introduced by RFNNS are not distributed globally but are instead concentrated in regions of high texture complexity. As a result, the overall range of the perturbation is effectively reduced, partially compromising the accuracy with which secret information can be extracted.

4.3.2 *Robustness with attack conditions.* The stego image transmitted over communication channels inevitably faces diverse and unpredictable interference. These attacks can compromise the accuracy of secret information extraction, thereby undermining the practical reliability of covert communication systems. In this section, we conduct a comprehensive evaluation of the robustness of existing FNNS methods against three common image attacks: JPEG compression, Gaussian noise, and contrast adjustment.

Under the low capacity condition, the proposed method outperforms the existing FNNS approach in all attack scenarios considered. This performance improvement can be attributed to the

implementation of the RSPG strategy, which incorporates common image attack scenarios into each iteration cycle during perturbation optimization. This significantly enhances the robustness of the perturbations, enabling more accurate decoding of the secret images.

Under the high capacity condition, RFNNS consistently outperforms the existing FNNS method in recovering secret images across various attack scenarios. In particular, under Gaussian noise of varying intensities, our method achieves an average improvement of approximately 4 dB in PSNR compared to other approaches. Moreover, across all tested scenarios of contrast adjustment attacks, our approach outperforms existing methods by an average of approximately 15 dB in terms of PSNR, yields an average SSIM improvement of around 2-fold, and obtains an LPIPS value that is only 6% of that achieved by SOTA methods. These notable improvements stem from the RSPG strategy, which exclusively focuses on local regions characterized by high texture complexity, enabling more effective fitting of robust perturbations. In contrast, the method proposed by Li et al. [28] employs global perturbations uniformly applied to the entire cover image, thus restricting its potential to effectively enhance robustness. Additionally, the approach of Li et al. incorporates simulated attacks only once every two optimization iterations, leading to unstable optimization loss and, consequently, hindering convergence toward robust perturbations.

5 Conclusion

In this paper, we propose a Robust Fixed Neural Network Steganography (RFNNS) that combines robust perturbations carrying secret information with AI-generated cover images to produce stego images. The introduced texture-aware localization technique effectively enhances the security of steganography. Additionally, a designed robust steganographic perturbation generation (RSPG)

strategy provides significant robustness against various common image attacks. Experimental results demonstrate the superiority of the proposed method under both low and high embedding capacities.

Acknowledgments

To Robert, for the bagels and explaining CMYK and color spaces.

References

- [1] Nasir Ahmed, T. Natarajan, and Kamisetty R Rao. 2006. Discrete cosine transform. *IEEE transactions on Computers* 100, 1 (2006), 90–93.
- [2] Shumeet Baluja. 2017. Hiding images in plain sight: Deep steganography. *Advances in neural information processing systems* 30 (2017).
- [3] Benedikt Boehm. 2014. Stegexpose-A tool for detecting LSB steganography. *arXiv preprint arXiv:1410.6656* (2014).
- [4] Mehdi Boroumand, Mo Chen, and Jessica Fridrich. 2018. Deep residual network for steganalysis of digital images. *IEEE Transactions on Information Forensics and Security* 14, 5 (2018), 1181–1193.
- [5] Tom Brown, Benjamin Mann, Nick Ryder, Melanie Subbiah, Jared D Kaplan, Prafulla Dhariwal, Arvind Neelakantan, Pranav Shyam, Girish Sastry, Amanda Askell, et al. 2020. Language models are few-shot learners. *Advances in neural information processing systems* 33 (2020), 1877–1901.
- [6] Chi-Kwong Chan and Lee-Ming Cheng. 2004. Hiding data in images by simple LSB substitution. *Pattern recognition* 37, 3 (2004), 469–474.
- [7] Haoyu Chen, Linqi Song, Zhenxing Qian, Xinpeng Zhang, and Kede Ma. 2022. Hiding images in deep probabilistic models. *Advances in Neural Information Processing Systems* 35 (2022), 36776–36788.
- [8] Yu Cheng, Zhenlin Luo, and Zhaoxia Yin. 2025. Robust steganography with boundary-preserving overflow alleviation and adaptive error correction. *Expert Systems with Applications* (2025), 127598.
- [9] Radoslaw M Cichy and Daniel Kaiser. 2019. Deep neural networks as scientific models. *Trends in cognitive sciences* 23, 4 (2019), 305–317.
- [10] Tomáš Filler, Jan Judas, and Jessica Fridrich. 2011. Minimizing additive distortion in steganography using syndrome-trellis codes. *IEEE Transactions on Information Forensics and Security* 6, 3 (2011), 920–935.
- [11] Georgi Ganev, Kai Xu, and Emiliano De Cristofaro. 2024. Graphical vs. Deep Generative Models: Measuring the Impact of Differentially Private Mechanisms and Budgets on Utility. In *Proceedings of the 2024 ACM SIGSAC Conference on Computer and Communications Security*. 1596–1610.
- [12] Salah Ghamizi, Maxime Cordy, Mike Papadakis, and Yves Le Traon. 2021. Evasion attack steganography: Turning vulnerability of machine learning to adversarial attacks into a real-world application. In *Proceedings of the IEEE/CVF International conference on computer vision*. 31–40.
- [13] Ian J Goodfellow, Jean Pouget-Abadie, Mehdi Mirza, Bing Xu, David Warde-Farley, Sherjil Ozair, Aaron Courville, and Yoshua Bengio. 2014. Generative adversarial nets. *Advances in neural information processing systems* 27 (2014).
- [14] Zhenyu Guan, Junpeng Jing, Xin Deng, Mai Xu, Lai Jiang, Zhou Zhang, and Yipeng Li. 2022. DeepMIH: Deep invertible network for multiple image hiding. *IEEE Transactions on Pattern Analysis and Machine Intelligence* 45, 1 (2022), 372–390.
- [15] Jonathan Ho, Ajay Jain, and Pieter Abbeel. 2020. Denoising diffusion probabilistic models. *Advances in neural information processing systems* 33 (2020), 6840–6851.
- [16] Jonathan Ho, Chitwan Saharia, William Chan, David J Fleet, Mohammad Norouzi, and Tim Salimans. 2022. Cascaded diffusion models for high fidelity image generation. *Journal of Machine Learning Research* 23, 47 (2022), 1–33.
- [17] Vojtěch Holub and Jessica Fridrich. 2012. Designing steganographic distortion using directional filters. In *2012 IEEE International workshop on information forensics and security (WIFS)*. IEEE, 234–239.
- [18] Vojtěch Holub and Jessica Fridrich. 2013. Digital image steganography using universal distortion. In *Proceedings of the first ACM workshop on Information hiding and multimedia security*. 59–68.
- [19] Dongxia Huang, Weiqi Luo, Minglin Liu, Weixuan Tang, and Jiwu Huang. 2023. Steganography embedding cost learning with generative multi-adversarial network. *IEEE Transactions on Information Forensics and Security* 19 (2023), 15–29.
- [20] Junpeng Jing, Xin Deng, Mai Xu, Jianyi Wang, and Zhenyu Guan. 2021. Hinet: Deep image hiding by invertible network. In *Proceedings of the IEEE/CVF international conference on computer vision*. 4733–4742.
- [21] Durk P Kingma and Prafulla Dhariwal. 2018. Glow: Generative flow with invertible 1x1 convolutions. *Advances in neural information processing systems* 31 (2018).
- [22] Diederik P Kingma, Max Welling, et al. 2013. Auto-encoding variational bayes.
- [23] Varsha Kishore, Xiangyu Chen, Yan Wang, Boyi Li, and Kilian Q Weinberger. 2021. Fixed neural network steganography: Train the images, not the network. In *International conference on learning representations*.
- [24] Meike Helena Kombrink, Zeno Jean Marius Hubert Geradts, and Marcel Worring. 2024. Image steganography approaches and their detection strategies: A survey. *Comput. Surveys* 57, 2 (2024), 1–40.
- [25] Leshan Lai, Yuansheng Liu, Bosheng Song, Keqin Li, and Xiangxiang Zeng. 2025. Deep Generative Models for the Therapeutic Peptide Discovery: A Comprehensive Review. *Comput. Surveys* (2025).
- [26] Bin Li, Ming Wang, Jiwu Huang, and Xiaolong Li. 2014. A new cost function for spatial image steganography. In *2014 IEEE International conference on image processing (ICIP)*. IEEE, 4206–4210.
- [27] Guobiao Li, Sheng Li, Zicong Luo, Zhenxing Qian, and Xinpeng Zhang. 2024. Purified and unified steganographic network. In *Proceedings of the IEEE/CVF conference on computer vision and pattern recognition*. 27569–27578.
- [28] Guobiao Li, Sheng Li, Zhenxing Qian, and Xinpeng Zhang. 2024. Cover-separable Fixed Neural Network Steganography via Deep Generative Models. In *Proceedings of the 32nd ACM International Conference on Multimedia*. 10238–10247.
- [29] Tsung-Yi Lin, Michael Maire, Serge Belongie, James Hays, Pietro Perona, Deva Ramanan, Piotr Dollár, and C Lawrence Zitnick. 2014. Microsoft coco: Common objects in context. In *Computer vision—ECCV 2014: 13th European conference, Zurich, Switzerland, September 6–12, 2014, proceedings, part v 13*. Springer, 740–755.
- [30] Weizhi Liu, Yue Li, Dongdong Lin, Hui Tian, and Haizhou Li. 2024. GROOT: Generating Robust Watermark for Diffusion-Model-Based Audio Synthesis. In *Proceedings of the 32nd ACM International Conference on Multimedia*. 3294–3302.
- [31] Ziwei Liu, Ping Luo, Xiaoqiang Wang, and Xiaoou Tang. 2015. Deep learning face attributes in the wild. In *Proceedings of the IEEE international conference on computer vision*. 3730–3738.
- [32] Zicong Luo, Sheng Li, Guobiao Li, Zhenxing Qian, and Xinpeng Zhang. 2023. Securing fixed neural network steganography. In *Proceedings of the 31st ACM international conference on multimedia*. 7943–7951.
- [33] Xueying Mao, Xiaoxiao Hu, Wanli Peng, Zhenliang Gan, Zhenxing Qian, Xinpeng Zhang, and Sheng Li. 2024. From covert hiding to visual editing: robust generative video steganography. In *Proceedings of the 32nd ACM International Conference on Multimedia*. 2757–2765.
- [34] Laijin Meng, Xinghao Jiang, Qiang Xu, and Tanfeng Sun. 2025. A Robust Coverless Video Steganography Based on Two-level DCT Features Against Video Attacks. *IEEE Transactions on Multimedia* (2025).
- [35] Timo Ojala, Matti Pietikainen, and Topi Maenpaa. 2002. Multiresolution gray-scale and rotation invariant texture classification with local binary patterns. *IEEE Transactions on pattern analysis and machine intelligence* 24, 7 (2002), 971–987.
- [36] Feng Pan, Jun Li, and Xiaoyuan Yang. 2011. Image steganography method based on PVD and modulus function. In *2011 International Conference on Electronics, Communications and Control (ICECC)*. IEEE, 282–284.
- [37] Yinyin Peng, Yaofei Wang, Donghui Hu, Kejiang Chen, Xianjin Rong, and Weiming Zhang. 2024. LDStega: Practical and Robust Generative Image Steganography based on Latent Diffusion Models. In *Proceedings of the 32nd ACM International Conference on Multimedia*. 3001–3009.
- [38] Matti Pietikäinen. 2010. Local binary patterns. *Scholarpedia* 5, 3 (2010), 9775.
- [39] Robin Rombach, Andreas Blattmann, Dominik Lorenz, Patrick Esser, and Björn Ommer. 2022. High-resolution image synthesis with latent diffusion models. In *Proceedings of the IEEE/CVF conference on computer vision and pattern recognition*. 10684–10695.
- [40] Olga Russakovsky, Jia Deng, Hao Su, Jonathan Krause, Sanjeev Satheesh, Sean Ma, Zhiheng Huang, Andrej Karpathy, Aditya Khosla, Michael Bernstein, et al. 2015. Imagenet large scale visual recognition challenge. *International journal of computer vision* 115 (2015), 211–252.
- [41] Martin Steinebach. 2024. Natural Language Steganography by ChatGPT. In *Proceedings of the 19th International Conference on Availability, Reliability and Security*. 1–9.
- [42] Christian Szegedy, Wojciech Zaremba, Ilya Sutskever, Joan Bruna, Dumitru Erhan, Ian Goodfellow, and Rob Fergus. 2013. Intriguing properties of neural networks. *arXiv preprint arXiv:1312.6199* (2013).
- [43] Weixuan Tang, Haoyu Yang, Yuan Rao, Zhili Zhou, and Fei Peng. 2024. Dig a Hole and Fill in Sand: Adversary and Hiding Decoupled Steganography. In *Proceedings of the 32nd ACM International Conference on Multimedia*. 10440–10448.
- [44] Jinyuan Tao, Sheng Li, Xinpeng Zhang, and Zichi Wang. 2018. Towards robust image steganography. *IEEE Transactions on Circuits and Systems for Video Technology* 29, 2 (2018), 594–600.
- [45] Tianyi Wang, Mengxiao Huang, Harry Cheng, Xiao Zhang, and Zhiqi Shen. 2024. LampMark: Proactive Deepfake Detection via Training-Free Landmark Perceptual Watermarks. In *Proceedings of the 32nd ACM International Conference on Multimedia*. 10515–10524.
- [46] Ping Wei, Sheng Li, Xinpeng Zhang, Ge Luo, Zhenxing Qian, and Qing Zhou. 2022. Generative steganography network. In *Proceedings of the 30th ACM International Conference on Multimedia*. 1621–1629.
- [47] Andreas Westfeld. 2001. F5—a steganographic algorithm: High capacity despite better steganalysis. In *International workshop on information hiding*. Springer, 289–302.
- [48] Jiaxuan Wu, Zhengxian Wu, Yiming Xue, Juan Wen, and Wanli Peng. 2024. Generative text steganography with large language model. In *Proceedings of the 32nd ACM International Conference on Multimedia*. 10345–10353.
- [49] Jian Ye, Jiangqun Ni, and Yang Yi. 2017. Deep learning hierarchical representations for image steganalysis. *IEEE Transactions on Information Forensics and Security* 12, 11 (2017), 2545–2557.

- [50] Huang Yi, Sun Shiyu, Duan Xiusheng, and Chen Zhigang. 2016. A study on deep neural networks framework. In *2016 IEEE advanced information management, communicates, electronic and automation control conference (IMCEC)*. IEEE, 1519–1522.
- [51] Weike You, Hong Zhang, and Xianfeng Zhao. 2020. A Siamese CNN for image steganalysis. *IEEE Transactions on Information Forensics and Security* 16 (2020), 291–306.
- [52] Zhuowen Yuan, Zhengxin You, Sheng Li, Zhenxing Qian, Xinpeng Zhang, and Alex Kot. 2022. On generating identifiable virtual faces. In *Proceedings of the 30th ACM International Conference on Multimedia*. 1465–1473.
- [53] Kai Zeng, Kejiang Chen, Weiming Zhang, Yaofei Wang, and Nenghai Yu. 2023. Robust steganography for high quality images. *IEEE Transactions on Circuits and Systems for Video Technology* 33, 9 (2023), 4893–4906.
- [54] Xiangxiang Zeng, Fei Wang, Yuan Luo, Seung-gu Kang, Jian Tang, Felice C Lightstone, Evandro F Fang, Wendy Cornell, Ruth Nussinov, and Feixiong Cheng. 2022. Deep generative molecular design reshapes drug discovery. *Cell Reports Medicine* 3, 12 (2022).
- [55] Kai Zhang, Wangmeng Zuo, Yunjin Chen, Deyu Meng, and Lei Zhang. 2017. Beyond a gaussian denoiser: Residual learning of deep cnn for image denoising. *IEEE transactions on image processing* 26, 7 (2017), 3142–3155.
- [56] Kevin Alex Zhang, Alfredo Cuesta-Infante, Lei Xu, and Kalyan Veeramachaneni. 2019. SteganoGAN: High capacity image steganography with GANs. *arXiv preprint arXiv:1901.03892* (2019).
- [57] Hongyu Zhu, Sichu Liang, Wentao Hu, Li Fangqi, Ju Jia, and Shi-Lin Wang. 2024. Reliable Model Watermarking: Defending Against Theft without Compromising on Evasion. In *Proceedings of the 32nd ACM International Conference on Multimedia*. 10124–10133.
- [58] Jiren Zhu, Russell Kaplan, Justin Johnson, and Li Fei-Fei. 2018. Hidden: Hiding data with deep networks. In *Proceedings of the European conference on computer vision (ECCV)*. 657–672.

A Ablation Experiment

A.1 Settings

To validate the effectiveness of RFNNS, we conduct an ablation study in this section to systematically analyze the contributions of the texture-aware localization technique and the robust steganographic perturbation generation (RSPG) strategy to the proposed method. The experimental settings are the same as those in Section 4.1.

A.2 Ablation Experiment 1: Texture-aware Localization

In this section, we conduct an ablation study, referred to as Ablation Experiment 1, in which the full RFNNS method is compared with a method that excludes the texture-aware localization technique. As shown in Table 4 and Table 5, when the texture-aware localization technique is not used, the visual quality of the secret images extracted remains largely unchanged, while the quality of the stego images decreases significantly. In addition, as shown in Fig. 6, the anti-steganalysis performance of the generated stego images is considerably lower than that of the RFNNS method. Specifically, omitting the texture-aware localization technique leads to a pronounced decrease in the quality of the stego image with respect to imperceptibility, accompanied by a substantial reduction in anti-steganalysis performance. This is due to the texture-aware localization technique, which divides the cover image into blocks, assesses their texture complexity, and selects appropriate regions for perturbation to maintain visual quality. Although employing this technique results in a slight decrease in robustness, its performance gap relative to the ablation method remains minimal. Given that security is the most important guarantee for covert communication, we consider the minor trade-off in robustness to be entirely acceptable.

A.3 Ablation Experiment 2: Robust Steganographic Perturbation Generation

In this section, we conduct an ablation study, referred to as Ablation Experiment 2, in which the full RFNNS method is compared with a method that excludes the robust steganographic perturbation generation (RSPG) strategy. As shown in Table 6 and Table 7, the visual quality of the stego images is approximately comparable to that of RFNNS, while the quality of the secret images extracted deteriorates significantly. Specifically, the RSPG strategy progressively reduces the discrepancy between the recovered and original secret images during the iterative optimization of the perturbations. In each optimization iteration, it introduces simulated image attack scenarios, which substantially enhances the robustness of the resulting stego images. Although employing this strategy entails a minor decline in stego image quality, it guarantees a commendable level of robustness. Under the low embedding capacity condition and in all contrast adjustments evaluated, the average PSNR of the recovered secret images increases by 6 dB, while the LPIPS value is only 20% of that achieved by the comparison methods. Under the high embedding capacity, and across all evaluated Gaussian noise attacks, the SSIM of the recovered secret images increases by

approximately 35%. Through this ablation experiment, the remarkable enhancement of robustness brought about by the proposed RSPG strategy is validated.

A.4 Conclusion of Ablation Experiment

Based on the ablation experiments, the following conclusions can be drawn: The texture-aware localization technique enhances the visual quality and steganalysis resistance of stego images by embedding perturbations carrying secret information into regions of high textural complexity, which are less perceptible to the human eye. Meanwhile, the robust steganographic perturbation generation (RSPG) strategy improves the quality of secret image extraction by simulating potential attack scenarios during the perturbation optimization process. This proactive approach mitigates extraction distortion caused by common image attacks, enabling the recovery of high-quality secret images even under adverse conditions.

The RFNNS method effectively integrates the strengths of the texture-aware localization technique and the RSPG strategy, achieving balanced optimization in terms of image quality, anti-steganalysis performance, and robustness, thus providing a more reliable and practical steganographic solution for real-world applications.

Table 4: Ablation Experiment 1: Stego Image Quality under Different Embedding Capacities and Attack Conditions

Capacity	Attack	Factor	RFNNS without the Texture-aware Localization			RFNNS		
			PSNR \uparrow	SSIM \uparrow	LPIPS \downarrow	PSNR \uparrow	SSIM \uparrow	LPIPS \downarrow
1.5bpp	No Attack		30.01	0.837	0.054	41.48	0.980	0.003
	JPEG Compression	$QF=90$	22.18	0.527	0.229	25.95	0.717	0.134
		$QF=80$	19.75	0.425	0.328	25.43	0.703	0.147
		$QF=70$	18.14	0.360	0.411	22.51	0.608	0.223
	Gaussian Noise	$\rho=0.01$	29.66	0.815	0.067	32.33	0.880	0.046
		$\rho=0.04$	24.40	0.632	0.169	28.66	0.800	0.089
		$\rho=0.07$	22.38	0.552	0.232	26.72	0.748	0.124
	Contrast Adjustment	$\eta=0.9$	30.03	0.836	0.054	33.46	0.913	0.041
		$\eta=0.8$	30.02	0.834	0.055	32.98	0.899	0.043
		$\eta=0.7$	29.95	0.832	0.055	32.60	0.889	0.047
6bpp	No Attack		30.01	0.835	0.041	42.95	0.984	0.003
	JPEG Compression	$QF=90$	17.23	0.327	0.357	22.62	0.583	0.218
		$QF=80$	16.65	0.304	0.410	21.58	0.565	0.222
		$QF=70$	16.36	0.293	0.434	19.81	0.522	0.292
	Gaussian Noise	$\rho=0.01$	27.48	0.743	0.085	31.62	0.864	0.048
		$\rho=0.04$	22.34	0.550	0.199	28.51	0.786	0.087
		$\rho=0.07$	20.53	0.477	0.251	26.19	0.738	0.130
	Contrast Adjustment	$\eta=0.9$	29.90	0.823	0.044	32.73	0.908	0.043
		$\eta=0.8$	28.65	0.787	0.056	30.72	0.845	0.059
		$\eta=0.7$	25.79	0.697	0.094	28.15	0.784	0.093

Table 5: Ablation Experiment 1: Recovered Secret Image Quality under Different Embedding Capacities and Attack Conditions

Capacity	Attack	Factor	RFNNS without the Texture-aware Localization			RFNNS		
			PSNR \uparrow	SSIM \uparrow	LPIPS \downarrow	PSNR \uparrow	SSIM \uparrow	LPIPS \downarrow
1.5bpp	No Attack		39.56	0.980	0.004	34.14	0.943	0.017
	JPEG Compression	$QF=90$	31.52	0.906	0.037	29.28	0.861	0.070
		$QF=80$	29.70	0.880	0.053	29.27	0.858	0.072
		$QF=70$	27.93	0.853	0.068	27.00	0.813	0.112
	Gaussian Noise	$\rho=0.01$	34.34	0.942	0.021	32.04	0.920	0.037
		$\rho=0.04$	30.82	0.892	0.048	27.44	0.816	0.124
		$\rho=0.07$	29.12	0.860	0.068	26.08	0.756	0.169
	Contrast Adjustment	$\eta=0.9$	40.17	0.981	0.003	34.62	0.968	0.016
		$\eta=0.8$	40.16	0.980	0.003	34.38	0.953	0.017
		$\eta=0.7$	40.02	0.977	0.003	33.68	0.950	0.019
6bpp	No Attack		38.56	0.963	0.009	31.09	0.910	0.058
	JPEG Compression	$QF=90$	22.26	0.760	0.184	23.60	0.720	0.253
		$QF=80$	20.20	0.706	0.248	22.85	0.696	0.260
		$QF=70$	19.00	0.667	0.296	19.24	0.572	0.411
	Gaussian Noise	$\rho=0.01$	32.43	0.902	0.051	30.07	0.855	0.117
		$\rho=0.04$	27.93	0.827	0.107	26.94	0.751	0.203
		$\rho=0.07$	25.00	0.776	0.153	24.49	0.665	0.294
	Contrast Adjustment	$\eta=0.9$	37.25	0.952	0.011	32.79	0.919	0.030
		$\eta=0.8$	33.76	0.933	0.021	30.67	0.898	0.043
		$\eta=0.7$	30.53	0.912	0.039	28.69	0.879	0.071

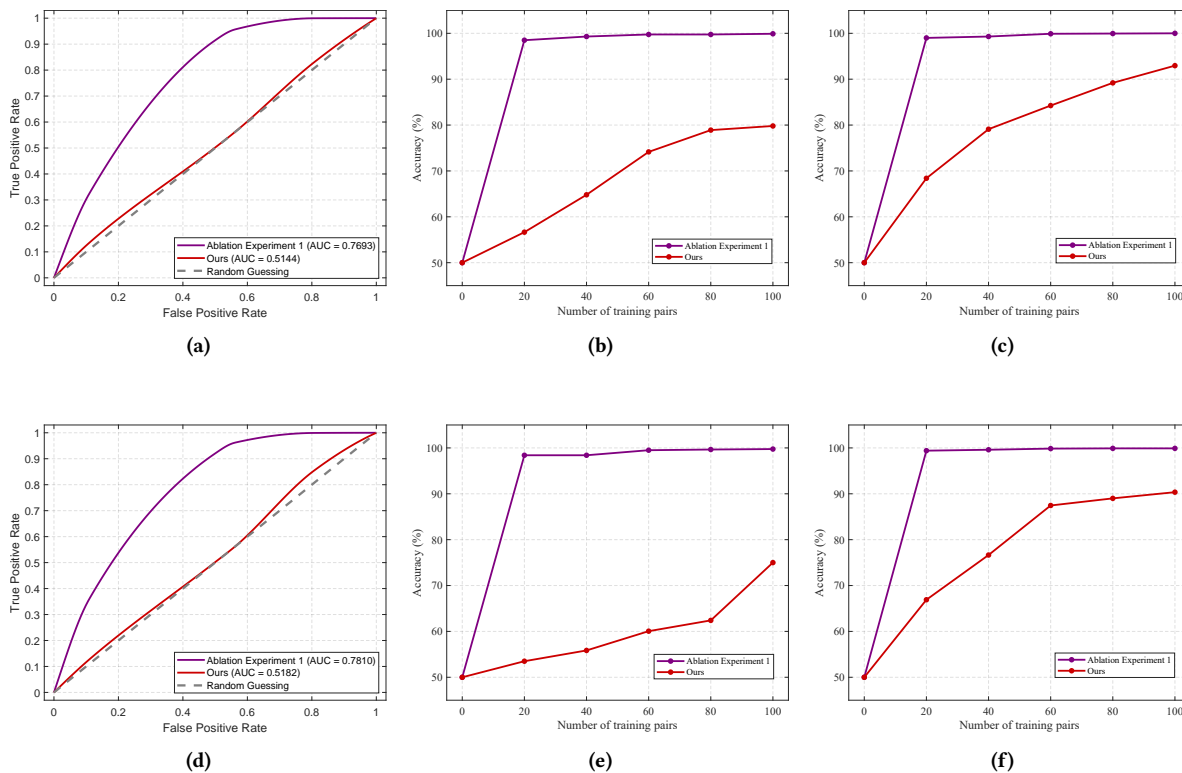


Figure 6: Ablation Experiment 1: The anti-steganalysis performance of the stego images generated using different methods against (a) (d) StegExpose, (b) (e) YeNet and (c) (f) SiaStegNet. The top row represents low embedding capacity (1.5 bpp), while the bottom row represents high embedding capacity (6 bpp).

Table 6: Ablation Experiment 2: Stego Image Quality under Different Embedding Capacities and Attack Conditions

Capacity	Attack	Factor	RFNNS without the RSPG strategy			RFNNS		
			PSNR \uparrow	SSIM \uparrow	LPIPS \downarrow	PSNR \uparrow	SSIM \uparrow	LPIPS \downarrow
1.5bpp	No Attack		46.24	0.963	0.001	41.48	0.980	0.003
	JPEG Compression	$QF=90$	29.48	0.820	0.119	25.95	0.717	0.134
		$QF=80$	26.88	0.745	0.185	25.43	0.703	0.147
		$QF=70$	25.54	0.702	0.236	22.51	0.608	0.223
	Gaussian Noise	$\rho=0.01$	33.96	0.905	0.033	32.33	0.880	0.046
		$\rho=0.04$	26.04	0.680	0.140	28.66	0.800	0.089
		$\rho=0.07$	22.26	0.530	0.262	26.72	0.748	0.124
	Contrast Adjustment	$\eta=0.9$	31.35	0.924	0.020	33.46	0.913	0.041
		$\eta=0.8$	27.02	0.916	0.031	32.98	0.899	0.043
		$\eta=0.7$	22.92	0.866	0.066	32.60	0.889	0.047
6bpp	No Attack		47.31	0.979	0.001	42.95	0.984	0.003
	JPEG Compression	$QF=90$	26.20	0.719	0.198	22.62	0.583	0.218
		$QF=80$	24.78	0.673	0.247	21.58	0.565	0.222
		$QF=70$	24.10	0.650	0.276	19.81	0.522	0.292
	Gaussian Noise	$\rho=0.01$	32.56	0.879	0.043	31.62	0.864	0.048
		$\rho=0.04$	25.21	0.650	0.158	28.51	0.786	0.087
		$\rho=0.07$	21.80	0.509	0.281	26.19	0.738	0.130
	Contrast Adjustment	$\eta=0.9$	31.32	0.924	0.020	32.73	0.908	0.043
		$\eta=0.8$	25.63	0.852	0.056	30.72	0.845	0.059
		$\eta=0.7$	22.41	0.789	0.100	28.15	0.784	0.093

Table 7: Ablation Experiment 2: Recovered Secret Image Quality under Different Embedding Capacities and Attack Conditions

Capacity	Attack	Factor	RFNNS without the RSPG strategy			RFNNS		
			PSNR \uparrow	SSIM \uparrow	LPIPS \downarrow	PSNR \uparrow	SSIM \uparrow	LPIPS \downarrow
1.5bpp	No Attack		30.77	0.892	0.037	34.14	0.943	0.017
	JPEG Compression	$QF=90$	27.28	0.799	0.130	29.28	0.861	0.070
		$QF=80$	26.06	0.761	0.131	29.27	0.858	0.072
		$QF=70$	23.95	0.726	0.191	27.00	0.813	0.112
	Gaussian Noise	$\rho=0.01$	28.91	0.843	0.094	32.04	0.920	0.037
		$\rho=0.04$	23.53	0.661	0.272	27.44	0.816	0.124
		$\rho=0.07$	21.10	0.570	0.378	26.08	0.756	0.169
	Contrast Adjustment	$\eta=0.9$	15.44	0.412	0.606	34.62	0.968	0.016
		$\eta=0.8$	14.48	0.357	0.621	34.38	0.953	0.017
		$\eta=0.7$	13.86	0.331	0.636	33.68	0.950	0.019
6bpp	No Attack		28.97	0.837	0.107	31.09	0.910	0.058
	JPEG Compression	$QF=90$	20.21	0.598	0.390	23.60	0.720	0.253
		$QF=80$	18.95	0.543	0.454	22.85	0.696	0.260
		$QF=70$	17.89	0.497	0.511	19.24	0.572	0.411
	Gaussian Noise	$\rho=0.01$	26.57	0.748	0.227	30.07	0.855	0.117
		$\rho=0.04$	20.39	0.523	0.481	26.94	0.751	0.203
		$\rho=0.07$	17.78	0.422	0.605	24.49	0.665	0.294
	Contrast Adjustment	$\eta=0.9$	15.77	0.413	0.604	32.79	0.919	0.030
		$\eta=0.8$	14.63	0.360	0.660	30.67	0.898	0.043
		$\eta=0.7$	13.95	0.323	0.711	28.69	0.879	0.071